



# Fabrication of high-performance composite membranes based on hierarchically structured electrospun nanofiber substrates for pervaporation desalination

Dujian Qin, Rui Zhang<sup>\*\*</sup>, Bing Cao<sup>\*\*\*</sup>, Pei Li<sup>\*</sup>

College of Materials Science and Engineering, Beijing University of Chemical Technology, Beijing, 100029, China

## ARTICLE INFO

### Keywords:

Pervaporation desalination  
Thin film composite (TFC) membrane  
Electrospun nanofiber substrate  
Nanofiber cellulose  
Polyvinyl alcohol

## ABSTRACT

Electrospun polyacrylonitrile (PAN) nanofiber membrane was fabricated. The surface of the PAN nanofiber membrane was spray-coated with a hydrophobic paint or knife-casted with an ultra-fine nanofiber cellulose (NC) layer. This was to mitigate the problem of infiltration of the coating solution into the pores of the virgin PAN nanofiber membrane when preparing composite membranes. As a result, defect-free and thin PVA layers were successfully deposited onto the hydrophobic PAN nanofiber or NC-PAN nanofiber substrates by a spray-coating method. The thin film composite (TFC) PVA/NC-PAN membrane exhibited extraordinary pervaporation desalination properties. A water flux of  $238.7 \pm 4.1 \text{ kg/m}^2 \cdot \text{h}$  and a salt rejection above 99.8% were obtained using a 3.5 wt% NaCl solution as feed at 80 °C. This is the highest reported water flux of all the PV desalination membranes. Moreover, a high-water flux of  $103.1 \pm 5.8 \text{ kg/m}^2 \cdot \text{h}$  was observed using the composite membrane to desalinate a 20 wt% NaCl solution at 70 °C. The excellent desalination property of the PV composite membrane demonstrates a great potential for recycling brine solutions.

## 1. Introduction

Today, water shortage remains one of the main worldwide issues that hinders the social development. To solve this limitation, many researchers attempt to purify the freshwater from seawater, brackish water, or other wastewater sources using electro dialysis, membranes or thermally based separation technologies [1,2]. Among them, nearly 60% desalination market is occupied by reverse osmosis (RO) because of its advantages of the high-water quality, mediated equipment investment, and low energy consumption ( $2\text{--}4 \text{ kW h/m}^3$ ) [3]. Nevertheless, RO is incapable for desalinating concentrated brines due to the rapidly increased cost at high osmotic pressures ( $5.5\text{--}6.8 \text{ MPa}$ ) [4,5]. Alternatively, thermally driven processes such as multi-stage flashing or multi-effect distillation can treat concentrated brine water since the driving force is not sensitive to salt concentration of the feed. Whereas some problems of the severe equipment corrosion, high capital investment and energy consumption ( $7\text{--}27 \text{ kW h/m}^3$ ) limit their applications [6]. As a developing prosperous technology, pervaporation (PV) desalination has superiorities of good ability for treating high salinity water,

anti-fouling and simple equipment. Moreover, if utilizing low grade waste heat or renewable solar/geothermal energy, the energy cost of PV desalination can be decreased to the level of the higher end of RO process. Therefore, PV desalination shows a considerable potential to replace conventional technologies in desalination applications [7–9]. However, one of the top challenges that restricts PV desalination from industrial application still lies in the relatively low water flux comparing with the commercial RO membranes ( $30\text{--}60 \text{ kg/(m}^2 \cdot \text{h)}$ ).

Fabrication a thin-film composite (TFC) PV membrane with a highly porous substrate and a top thin selective layer (several-hundred nanometers) is an effective way to achieve the purpose of high-water flux [10]. According the solution-diffusion mechanism, water molecule first dissolves and then transfers to the bottom of the selective layer, and finally desorbs at the permeate side [8,13]. Because water permeates through the porous substrate of a PV composite membrane in gas state, whose volume is about thousand times larger than in liquid state, the vapor transfer resistance of the support layer of PV composite membrane plays an important role in determining the overall water flux [11]. In this work, two different kinds of membranes comprising PVDF and PAN

\* Corresponding author.

\*\* Corresponding author.

\*\*\* Corresponding author.

E-mail addresses: [zhangrui1@mail.buct.edu.cn](mailto:zhangrui1@mail.buct.edu.cn) (R. Zhang), [bcao@mail.buct.edu.cn](mailto:bcao@mail.buct.edu.cn) (B. Cao), [lpei@mail.buct.edu.cn](mailto:lpei@mail.buct.edu.cn) (P. Li).

<https://doi.org/10.1016/j.memsci.2021.119672>

Received 24 May 2021; Received in revised form 27 July 2021; Accepted 28 July 2021

Available online 30 July 2021

0376-7388/© 2021 Elsevier B.V. All rights reserved.

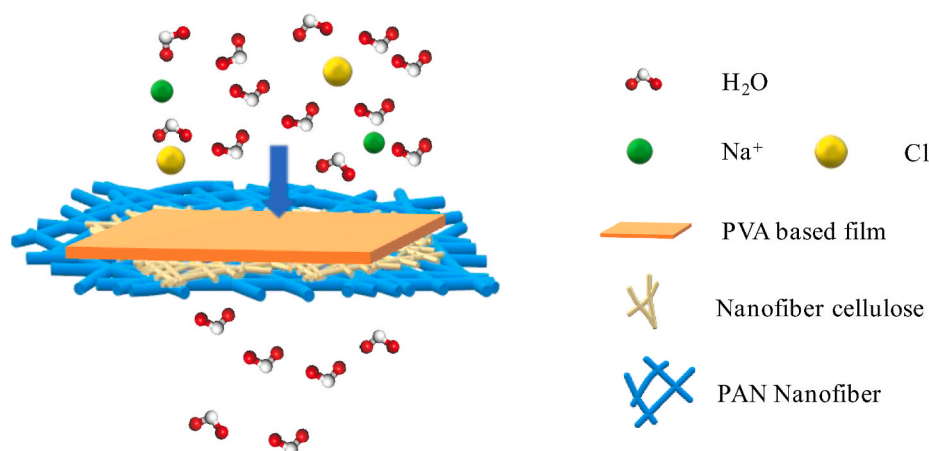


Fig. 1. Illustrations of the desalination process using the thin-film composites (TFC) membranes of PVA/NC-PAN.

electrospun nanofiber substrates are fabricated by the typical non-solvent induced phase inversion (NIPS) method and the electrospinning technique. Attributing to the dense skin layer and numerous dead-end pores though its cross-section [12], the NIPS membrane has a relatively high resistance, which is proved by a pressure build-up analysis in this study. While the electrospun nanofibrous membranes show less gas transport resistance due to the interconnected pores and highly porous surfaces morphology. Therefore, the PAN nanofibrous membranes are ideal supporting layers for preparing high flux TFC PV membranes [13]. However, directly depositing a thin selective layer ( $< 1 \mu\text{m}$ ) on the porous nanofibrous membrane top surface is not trivial attributing to the serious infiltration of the casting solution into the hydrophilic substrate with large surface pore size, and thus leads to the formation of defects on the membrane surface [14]. To address this limitation, many techniques have been adopted such as pre-crosslinking the coating polymer or filling the pores of the nanofiber substrate to minimize the penetration of the coating solution, or reducing the surface pore sizes of the electrospun nanofiber membrane [15–17]. These treatments are time-consuming or complicated.

The key factor for depositing a thin defect-free selective layer on an electrospun nanofiber substrates is to prevent the intrusion of the coating solution into the large surface pores of the substrates. In this work, two simple but efficient techniques are developed. One is to adjust the surface property of a PAN nanofiber membrane by painting a hydrophobic chemical agent. Then a relatively thick PVA ( $\sim 3.50 \mu\text{m}$ ) layer is deposited on top of the hydrophobically treated PAN nanofiber substrate. The other method is to build a transition layer between the PVA top layer and the PAN substrate to prevent the PVA intrusion. This is realized by knife-coating an ultra-fine nanofiber cellulose (NC) layer on the PAN nanofiber substrate (Fig. 5S). Because of the NC gutter layer, most PVA molecules are rejected, and thus a thin but defect-free PVA top layer ( $\sim 700 \text{ nm}$ ) can be deposited onto the NC-PAN substrate by a spray-coating method. Eventually, the thin-film composite (TFC) PV membrane is prepared successfully (Fig. 1). The TFC PV membrane exhibits water fluxes of  $153.4 \pm 3.4 \text{ kg}/(\text{m}^2\cdot\text{h})$  at  $70 \text{ }^\circ\text{C}$ , and  $238.7 \pm 4.1 \text{ kg}/(\text{m}^2\cdot\text{h})$  at  $80 \text{ }^\circ\text{C}$  with a salt rejection over 99.8% for desalinating a 3.5 wt % NaCl solution. Moreover, the water permeation flux reaches to  $103.1 \pm 5.8 \text{ kg}/(\text{m}^2\cdot\text{h})$  at  $70 \text{ }^\circ\text{C}$  using a 20 wt% NaCl solution as feed. Attributing to the optimized substrates and the thinner selective layer, this desalination property out-performs the highest reported data of all the PV desalination membranes [17–19]. More importantly, the facial fabrication method, and the excellent water production with high desalination performance, indicates great potential of the TFC PV membranes in treating high concentrated saline water.

## 2. Experimental

### 2.1. Materials

Polyethylene terephthalate (PET) non-woven (TER-80B MIKI TOKUSHU PAPER) was bought from MFG Co., Ltd. Poly(vinyl alcohol) (PVA, hydrolysis degree: 99.4%,  $M_w$ : 105,000), poly(vinylidene fluoride) (PVDF, purity  $\geq 99.5\%$ ,  $M_w$ : 200,000), and poly(4-styrenesulfonic acid-co-maleic acid) sodium salt (P(SS-MA),  $M_w$ : 20,000) were purchased from Sigma-Aldrich (USA). Poly(vinylpyrrolidone) (PVP K-30, purity  $\geq 95.0\%$ ,  $M_w$ : 50,000) was obtained from Gobekie Co., Ltd. N-methyl-2-pyrrolidone (NMP, purity  $\geq 99.0\%$ ), N, N-dimethylformamide (DMF, purity  $\geq 99.0\%$ ), 98% sulfuric acid ( $\text{H}_2\text{SO}_4$ ) and 35% hydrochloric acid solution (HCl) were purchased from Tianjin Damao Chemical Reagent Factory (China). Sodium chloride (NaCl, purity  $\geq 99.5\%$ ) and polyacrylonitrile (PAN,  $M_w$ : 150,000) were bought from Sinopharm Chemical Reagent Co., Ltd. (China). A water proof spray containing a perfluorinated solvent was bought from Guangzhou Xuwu Trading Co., Ltd. TEMPO oxidized nanofiber cellulose aqueous solution was purchased from Tianjin Wood Elves Biotechnology Co., Ltd. Deionized (DI) water was produced from a lab-equipped Millipore ultrapure water system with a conductivity of  $10.6 \mu\text{S}/\text{cm}$ .

### 2.2. Preparation of the PVA coating solution

First, a 0.5 wt% PVA aqueous solution and a 30 wt% P(SS-MA) water solution were prepared. Then, the 30 wt% P(SS-MA) solution was gradually added to the PVA solution till the weight ratio of PVA to P(SS-MA) reached to 8:2. The solution pH was turned to 1 by adding  $\text{H}_2\text{SO}_4$ .

### 2.3. Membrane fabrication

#### 2.3.1. Fabrication the PVDF membranes

The PVDF membranes were prepared via the non-solvent induced phase inversion (NIPS) method [20–22]. Specifically, a homogeneous polymer solution consisting of PVDF, PVP, and NMP in a weight ratio of 13/5/82 was cast onto a PET non-woven fabric using a  $150 \mu\text{m}$  casting-knife. The gel-like polymer film along with the PET fabric was immersed in a water bath at  $25 \text{ }^\circ\text{C}$  to form a porous PVDF membrane. The water bath was replaced for 2 times to remove the residual solvent in the membrane. At last, the water-wet PVDF membrane was dried by a solvent exchange method as introduced in a reference paper [23].

#### 2.3.2. Preparation of the electrospun PAN nanfiber membrane

PAN was dissolved in DMF at concentrations of 9 wt%, 10 wt%, 11 wt%, and 12 wt% for electrospinning. In all electrospinning processes, the applied voltage was 17–18 kV, and the PAN solution was fed to the

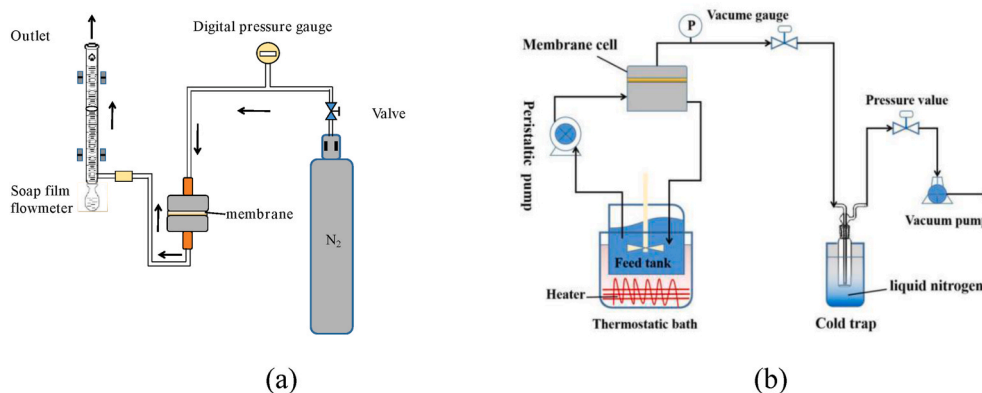


Fig. 2. Schematic diagrams of the process of gas resistance measurement of substrates (a) and the PV measurement for composite membranes (b).

electric field by a syringe equipped with a needle of 0.7 mm outer diameter at a rate of 10  $\mu\text{L}/\text{min}$ . The syringe was oscillated within a range of 30 cm in a translational motion perpendicular to the rotation direction of the collector. The nanofibers were collected by a drum covered with an aluminum foil at a rotating rate of 180 r/min. The distance between the needle and the drum was 24 cm. After electrospinning, the PAN nanofiber membranes with different concentration of PAN were obtained as shown in Fig. S2 in the supporting information. All the electrospinning processes were carried out at 20  $^{\circ}\text{C}$  with an air humidity of 20–30%.

### 2.3.3. Preparation of the NC-PAN composite membranes

A piece of electrospun PAN nanofiber membrane was immersed in a HCl solution (pH = 1.85) for 2 min. Then the membrane was fixed on a glass plate and excess water on the membrane surface was wiped off using a glass rod. Subsequently, a 0.5 wt% NC solution was cast on top of the wet nanofibrous membrane using a casting knife. After that, the NC-PAN composite membrane was air-dried for 2 h at 25  $^{\circ}\text{C}$  and then vacuum dried at 60  $^{\circ}\text{C}$  for 4 h. The NC layer thickness was controlled by a casting knife.

### 2.3.4. Preparation of the PV composite membranes

A PVA solution was spray-coated using an air-brush on the PVDF, hydrophobically treated PAN nanofiber, and NC-PAN nanofiber membranes to obtain the PV composite membranes. The spraying-coating method was detailed introduced in our previous study [24]. The spray-coating processes of the composites using the PVDF and PAN nanofiber membranes were described in the following paragraphs.

To prepare the PVA/PVDF composite membranes, the PVA solution was directly sprayed onto the PVDF membrane. Thicknesses of the PVA layers were controlled by controlling the spraying volumes.

To prepare the PVA/PAN nanofiber composite membranes, two techniques including hydrophobic modification of the PAN nanofiber surface and coating a NC gutter layer are adopted. Hydrophobic modification was done by spray-coating a hydrophobic paint onto the PAN nanofiber surface at a volume of 12.52  $\mu\text{L}/\text{cm}^2$ . This was to prevent the penetration of the atomized PVA solution droplets into the macroporous PAN nanofiber membrane. After the hydrophobic treatment, the defect-free PVA/PAN nanofiber composite membranes could be prepared at a lowest spray-coating volume of 163.27  $\mu\text{L}/\text{cm}^2$  of the PVA solution. For the NC coating method, surface pores sizes of the PAN nanofiber membrane were significantly reduced. Hence, the leaking problem of the PVA coating solution was solved. TFC membrane with thinner PVA layers were realized by reducing the spray-coating solution volumes from 163.27  $\mu\text{L}/\text{cm}^2$ , 65.31  $\mu\text{L}/\text{cm}^2$ , to 32.65  $\mu\text{L}/\text{cm}^2$ , corresponding to the PVA layer thicknesses of 3.78  $\mu\text{m}$ , 1.26  $\mu\text{m}$ , and 0.70  $\mu\text{m}$ , respectively. After coating, all the composite PV membranes were heated at 100  $^{\circ}\text{C}$  for 15 min to crosslink the PVA.

## 2.4. Membrane characterizations

### 2.4.1. Determination of the morphologies and hydrophilicity of the membranes

Cross-section and surface morphologies of composite membranes were characterized by a scanning electron microscope (SEM) (HITACHI S-7800 Japan). An image J software was used to calculate the average surface pore diameters and porosities of the PVDF, electrospun PAN nanofiber and NC-PAN composite according to their surface SEM images [25–27]. The layer thicknesses of the composite membranes were determined based on the cross-section SEM images using a Nano Measurer software.

Atomic Force Microscopy (AFM) (Dimension Fastscantm, Bruker, USA) was used to observe the surface morphology of the membranes. Contact angle goniometer (CA) (DSA100, KRUSS, Germany) was used to measure the water contact angles of the electrospun PAN nanofiber membrane, hydrophobically treated PAN nanofiber membrane and the PVA/hydrophobic PAN membrane. A 2  $\mu\text{L}$  water droplet was dropped on a membrane surface and a dynamic contact angle was determined using a high-speed optimum video analysis system. To acquire the dimension morphology of cellulose nanofiber, a transmission electron microscope (TEM) (FEI BioTwinG2), which equipped with an AMT digital camera, was operated at an accelerating voltage of 120 kV with goniometer tilt capability. Before measuring, the cellulose nanofiber aqueous suspension (0.01 wt %) was coated on a grid (Ted Pella) and followed by staining with uranyl acetate aqueous solution (2.0 wt %).

### 2.4.2. Separation tests of the PVDF, PAN nanofiber, hydrophobic treated PAN nanofiber and NC-PAN nanofiber membranes

The ultrafiltration performances of the membranes were carried out using a cross-flow ultrafiltration (UF) membrane module as shown in Fig. S7a in the supporting information, where the effective membrane area was 3.14  $\text{cm}^2$ . Initially, membrane was compacted at 0.2 MPa for 1 h till the water flux became stable. Then the water flux was measured at 0.1 MPa every 10 min for 3 times at room temperature. The flux was calculated by eq. (1):

$$J_{w1} = \frac{M}{A_1 \times T_1} \quad (1)$$

where  $J_{w1}$  was the permeate flux ( $\text{kg}/(\text{m}^2 \cdot \text{h})$ );  $A_1$  was the effective membrane area ( $\text{m}^2$ ); and  $T_1$  was the operation period (h). Rejection experiments were performed at 0.1 MPa using a 1 g/L PVA ( $M_w$ : 105,000) solution as feed. Concentrations of PVA was measured using a totally organic carbon (TOC) analysis (TOC-L, SHIMADZU, Japan). The calibration curve of TOC was provided in Fig. S7b in the supporting information. The solute rejection (R) of PVA was calculated by eq. (2):

$$R = \left( \frac{Cf_2 - Cp_2}{Cf_2} \right) \times 100\% \quad (2)$$

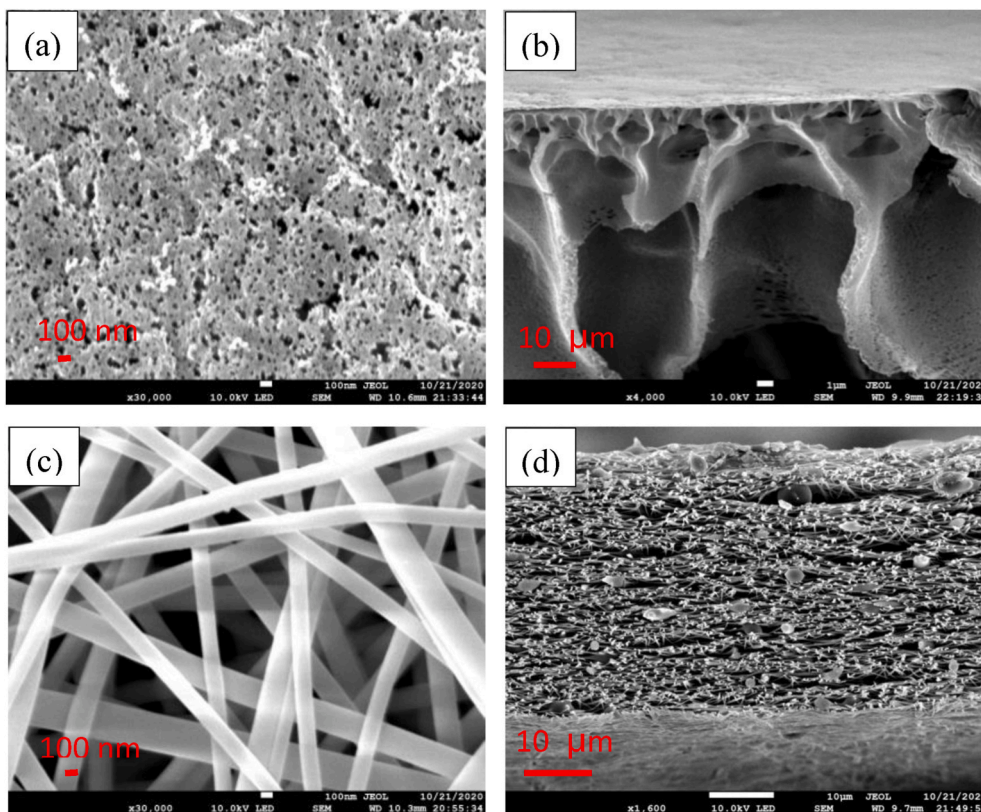


Fig. 3. SEM images of the surface and cross-section morphologies of PVDF (a,b) and the PAN electrospun nanofiber membranes (c,d).

where  $C_{p2}$  was concentration of the solute in permeate and  $C_{f2}$  was concentration of the solute in feed.

#### 2.4.3. Gas permeation tests of the PVDF, PAN nanofiber, hydrophobic treated PAN nanofiber and NC-PAN membranes

A gas permeation cell was used to correlate the relation between *trans*-membrane pressure and  $N_2$  flux to estimate the resistance of the membrane to water vapor transport (Fig. 2) [28].  $N_2$  flux was calculated by eq. (3):

$$Q = \frac{V}{A_2 \cdot T_2} \quad (3)$$

where  $Q$  was the  $N_2$  ( $L/(m^2 \cdot h)$ );  $V$  was the volume of the permeated gas ( $L$ );  $A_2$  was the effective membrane area ( $m^2$ ); and  $T_2$  is the permeation time ( $h$ ). A curve of  $Q$  vs.  $T_2$  was plotted and the slop of the curve was used to estimate the membrane resistance to gas transport.

#### 2.4.4. PV desalination tests

The desalination properties of the composite PV membranes were carried out using a laboratory PV set-up (Fig. 2), where the effective membrane area was  $3.28 \text{ cm}^2$ . Feed solution comprising 0–20 wt% NaCl were circulated though the PV cell at a flow rate from 0.1 m/s and membrane permeate side was vacuumed at 100 Pa. Water vapor was collected every 10 min for 3 times by a liquid nitrogen cold trap. The permeation flux were analyzed by eq. (4):

$$J_{w3} = \frac{M}{A_3 \times T_3} \quad (4)$$

where  $J_{w3}$  was the permeate flux ( $kg/m^2 \cdot h$ ),  $A_3$  was the effective membrane area ( $m^2$ ), and  $T_3$  was the operation period ( $h$ ). Solute concentrations of ions in the feed and permeate samples were analyzed by a DDSJ-308F electrical conductivity meter (Leichi, China). The salt rejection ( $R$ ) was determined using eq. 5

$$R = \left( \frac{C_{f3} - C_{p3}}{C_{f3}} \right) \times 100\% \quad (5)$$

where  $C_{p3}$  was the ion concentration in the permeate and  $C_{f3}$  was the ion concentration of in the feed.

#### 2.4.5. Estimation of the pressure build-up of water vapor on the interface between the dense layer and the porous supports by a resistance model

The pressure build-ups of water vapor at the interface between the top dense layer and the porous substrate were calculated by a resistance model [29]. The pressure build-up was analyzed by eq. (6) [30]:

$$F_w = K \times (P - 0.1) \quad (6)$$

where  $F_w$  is the water vapor flux ( $L/m^2 \cdot h$ );  $P$  is the pressure build-up in a unit of kPa; 0.1 is the vacuum side pressure of 100 Pa;  $K$  is the slope measured from the gas flux and the *trans*-membrane pressure.

## 3. Results and discussion

### 3.1. Characterization of PVDF and PAN support layers

Two kinds of support layers comprising PVDF and PAN electrospun nanofiber substrates are fabricated by the non-solvent induced phase inversion (NIPS) method and electrospinning technique, respectively. The SEM images in Fig. 3 demonstrate that both the surface and cross-section morphologies of the PVDF membrane and PAN electrospun nanofiber membrane. It can be clearly found that the NIPS PVDF membrane has a porous layer full of finger-like macro-voids and a relatively dense skin layer, which may lead to a high resistance to water vapor transport. Whereas an inter-connected porous structure without dense skin layer exists in the electrospun nanofiber membrane (a schematic diagram of electrospinning process can be found in Fig. S1 of the supporting information). Hence, the transport resistance of the

**Table 1**

The surface porosity and mean pore size of the PVDF and PAN nanofiber membranes.

Membrane	Surface porosity (%)	Mean pore size (nm)
PVDF	14.00 ± 1.52	13.65 ± 2.33
PAN nanofiber	22.97 ± 4.10	149.50 ± 6.80

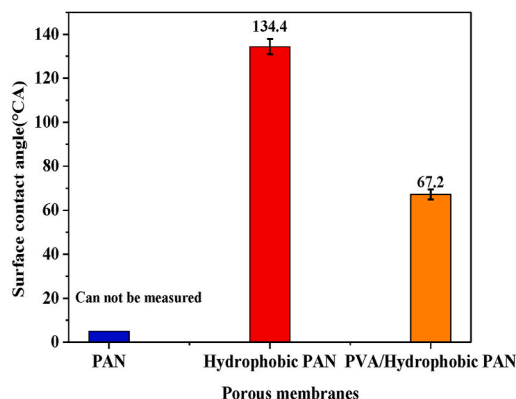
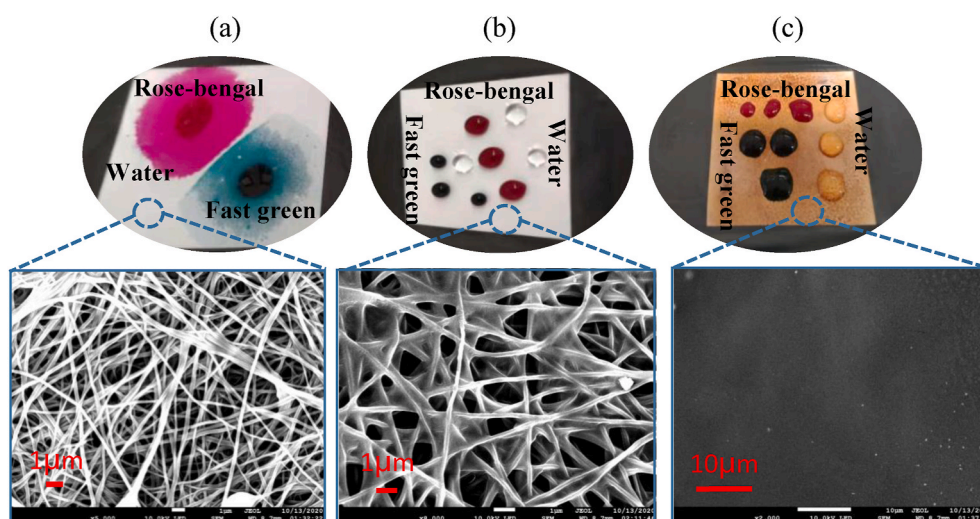
nanofiber membrane shall be much lower than the NIPS PVDF membrane.

Table 1 lists the surface mean pores size and the porosity of PVDF membrane which are  $13.65 \pm 2.33$  nm and  $14.00 \pm 1.52\%$ , respectively. While those of the PAN nanofiber membrane are  $149.50 \pm 6.80$  nm and  $22.97 \pm 4.10\%$ . The mean pores size and the porosity of the PAN electrospun nanofiber substrate increase by 10 times and 0.64 time, respectively. We directly spray-coat the PVA casting solution on the two membrane surfaces. It is easy to fabricate a thin selective layer ( $< 1 \mu\text{m}$ , Fig. 6a<sub>1</sub>) onto the PVDF membrane because of its smaller average pore size. However, the large surface pores make it difficult to deposit a defect-free layer on top of the PAN electrospun nanofiber membranes. Therefore, modification of the PAN nanofiber membrane is crucial for making the PVA/PAN composite PV membranes.

### 3.2. Modification of the PAN nanofiber membrane surface

Surface hydrophobicity plays an important role to expel water droplets out of membrane pores. To prevent the infiltration of PVA aqueous solution into the PAN nanofiber membrane, we spray a water proof paint on the nanofiber surface before depositing the PVA layer. Fig. 4a illustrates that the water and dye droplets spread on surface of the pristine PAN nanofiber membrane, indicating the hydrophilic nature of the PAN nanofibrous fiber. Therefore, when directly spray-coat a 0.5 wt% PVA solution onto the pristine PAN nanofiber membrane, the coating solution droplets immediately penetrates into the fibrous membranes as shown in supporting information of video 1. Therefore, a PVA/PAN nanofiber composite membrane with surface defects is obtained. However, after coating the fluorinated paint, a water contact angle of  $134.4^\circ$  is observed as shown in Fig. 4d, indicating that the surface of the PAN nanofiber membrane becomes hydrophobic. In addition, part of the surface pores is covered by the fluorinated paint as shown in Fig. 4b, indicating the successfully deposition of the hydrophobic paint. Therefore, a uniformly distributed PVA layer can form on top of the hydrophobically treated PAN nanofiber membrane by a simple spray-coating method as reported in Ref. [24]. After crosslinking the PVA layer, the water contact angle of the composite membrane decreases to  $67.2^\circ$ , indicating the hydrophilic nature of PVA layer.

Supplementary video related to this article can be found at <https>



(d)

**Fig. 4.** The SEM images of water and dyes solution on the membranes surface of pristine PAN (a); hydrophobic PAN(b); PVA/hydrophobic PAN(c) and water contact angles of the pristine PAN, hydrophobic PAN and PVA/hydrophobic PAN(d).

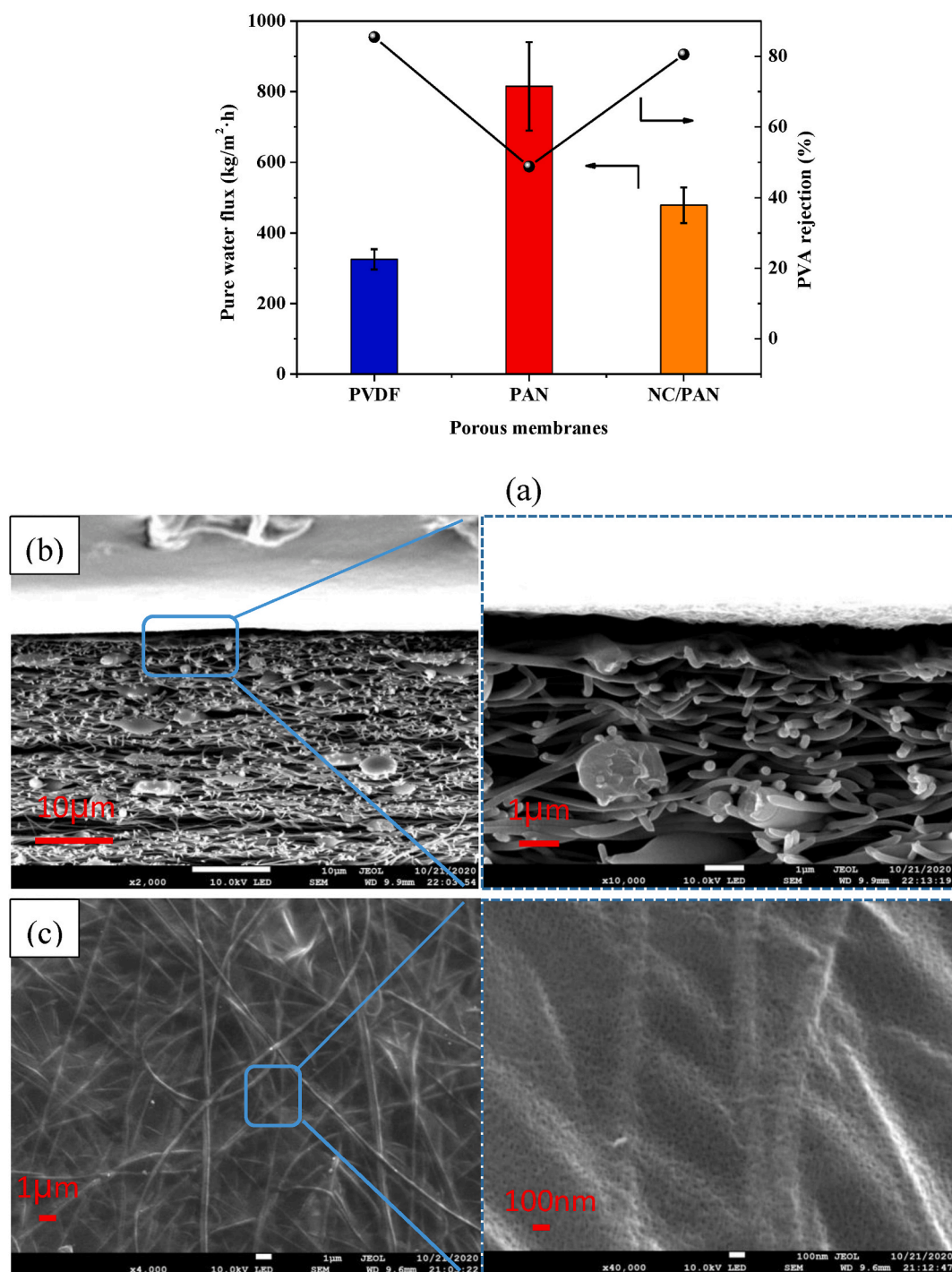


**Fig. 5.** Pure water flux and PVA rejection of PVDF, PAN and NC/PAN membranes(a), SEM images of NC/PAN support layers: cross-section (b) and the top surface morphologies(c).

[://doi.org/10.1016/j.memsci.2021.119672](https://doi.org/10.1016/j.memsci.2021.119672)

Reducing the surface pore size of the PAN nanofiber membrane is another way to alleviate the infiltration of the PVA coating solution. This is done by depositing a NC gutter layer onto the PAN nanofiber surface. As shown in the TEM image of Fig. S5a, the ultra-fine NC fibers have a diameter of 5–10 nm and a length of 200–400 nm [31–34]. The high aspect ratio characteristic of NC makes it an ideal material to form an ultra-thin transition layer on top of PAN nanofibrous membranes with marginal increment in transport resistant [35–37]. Fig. 5a illustrates that the rejection rate to PVA of the NC/PAN composite membrane is improved from 50.2% to 80.6%, which is similar to the rejection of the

PVDF membrane (85.4%) to PVA after depositing the NC aqueous solution onto PAN fibrous membrane surface (the casting process is illustrated in Fig. S5b). This is because the large surface pores of the pristine PAN nanofiber membrane (~149.50 nm) is reduced to ~22.71 nm by the ultra-thin NC layer (~107.6 nm). Therefore, a defect-free PVA layer can be deposited on the top surface of NC-PAN substrate (Fig. 6c).

### 3.3. Effect of the substrates' structures on PV performance

As shown in Fig. 6a, b, c, the defect-free crosslinked PVA layers of 0.88 μm, 3.50 μm and 3.78 μm are formed on the PVDF, hydrophobic

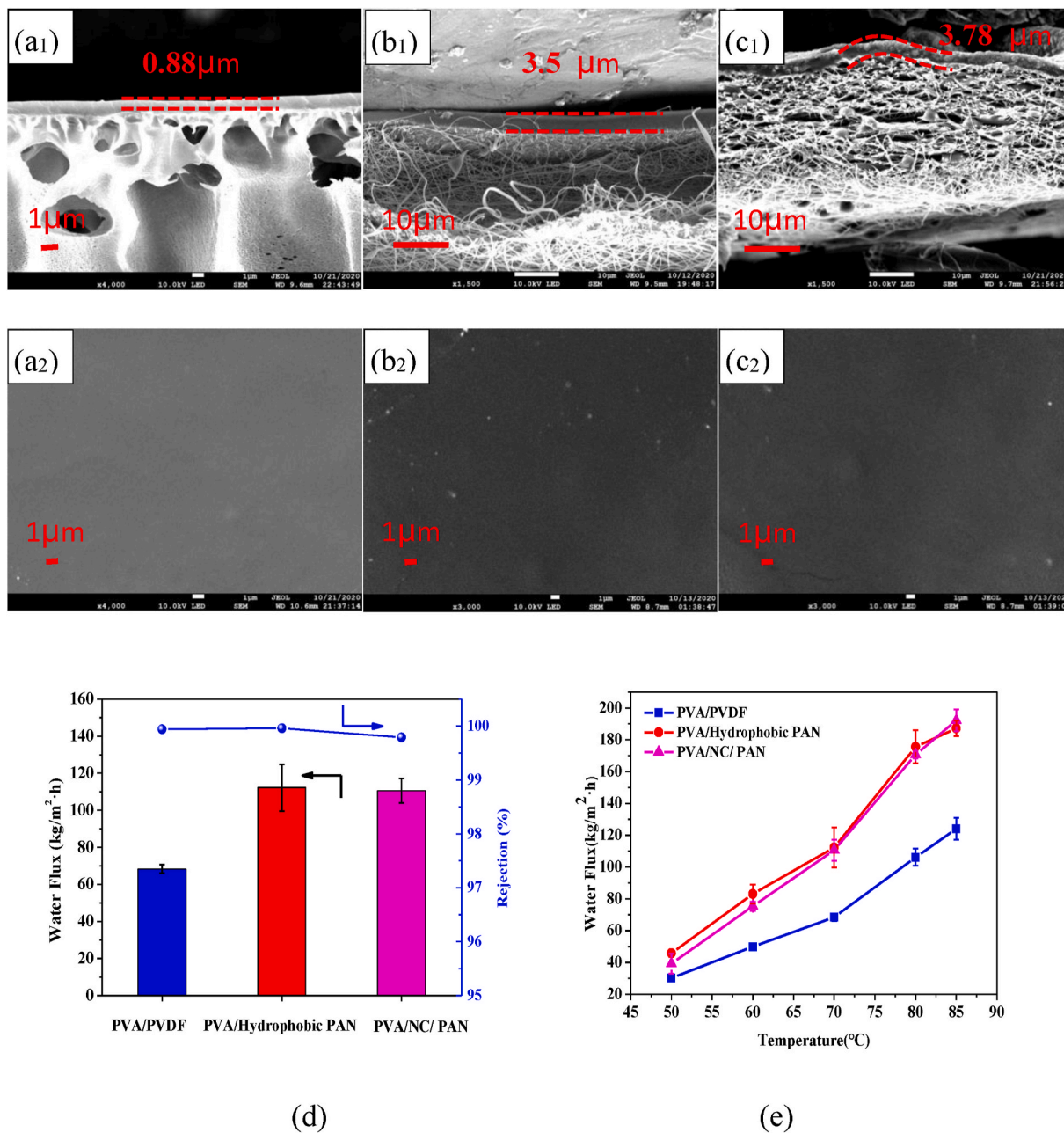


**Fig. 6.** The SEM images of the cross sectional and surface morphologies of PVA/PVDF(a<sub>1</sub>, a<sub>2</sub>), PVA/Hydrophobic PAN(b<sub>1</sub>,b<sub>2</sub>) and PVA/NC-PAN(c<sub>1</sub>,c<sub>2</sub>); the desalination properties at 70 °C(d) and water flux (e) from 50 °C to 85 °C of the PVA/PVDF, PVA/PAN and PVA/NC-PAN composite PV membranes using a 3.5 wt% NaCl solution as feed.

PAN nanofiber, and NC-PAN nanofiber membranes. Fig. 6d shows that all the composite membranes have a high salt rejection above 99.8% and the PVA/PVDF membrane has the lowest water flux of  $70.4 \pm 2.5$  kg/(m<sup>2</sup>·h) at 70 °C using a 3.5 wt% NaCl solution as feed, while the permeation fluxes of the PVA/hydrophobic PAN and PVA/NC-PAN membranes are  $112.3 \pm 12.6$  kg/(m<sup>2</sup>·h) and  $110.9 \pm 5.1$  kg/(m<sup>2</sup>·h), respectively. As the feed temperature increased from 50 °C to 85 °C, the water fluxes of the PVA/hydrophobic PAN and the PVA/NC-PAN composite membranes increase more rapidly than that of the PVA/PVDF membrane, demonstrating in Fig. 6e. Clearly, all the PAN nanofiber mat based composite membranes show better performance than that of PVDF based membrane. Liang et al. has reported that the water fluxes of PV composite membranes non-linearly decreased with the increment in the selective layers' thickness [30]. In this study, although the thicknesses of the PVA layers on the PAN nanofiber substrate are thicker than

that of the PVA/PVDF membrane, their water fluxes are higher. Therefore, we believe that the higher water fluxes result in the much lower resistances of the nanofiber substrates.

### 3.4. Resistance evaluation of the substrates

The substrate resistances of the PVDF, hydrophobic PAN nanofiber membrane and the NC-PAN nanofiber membrane are estimated by measuring their resistances to N<sub>2</sub> transport [38,39]. Fig. 7a Demonstrates that all the N<sub>2</sub> fluxes linearly increase with the *trans*-membrane pressure revealing that the gas transport behavior matches the character of viscosity flow. Fig. 7b shows that the hydrophobic PAN nanofiber membrane has the highest gas permeance ( $265.6 \times 10^5$  L/(m<sup>2</sup> h bar)), which is 11.7 times higher than that of PVDF membrane ( $22.7 \times 10^5$  L/(m<sup>2</sup> h bar)). After coating the NC layer, the gas permeance decreases to

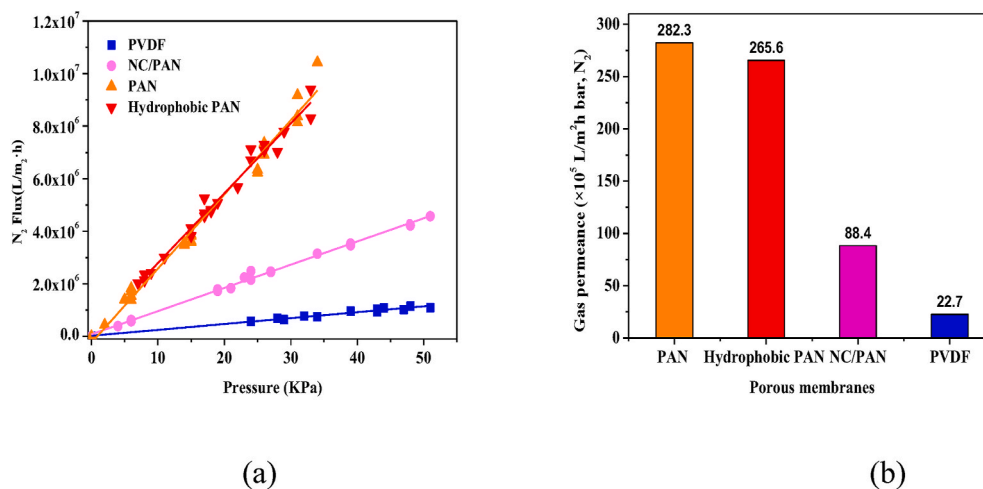


Fig. 7. Gas fluxes (a) and gas permeances (b) of the PVDF, PAN, Hydrophobic PAN and NC-PAN at different *trans*-membrane pressures.

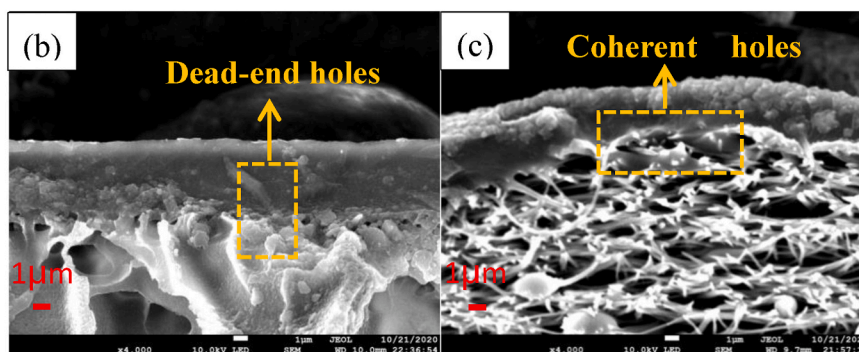
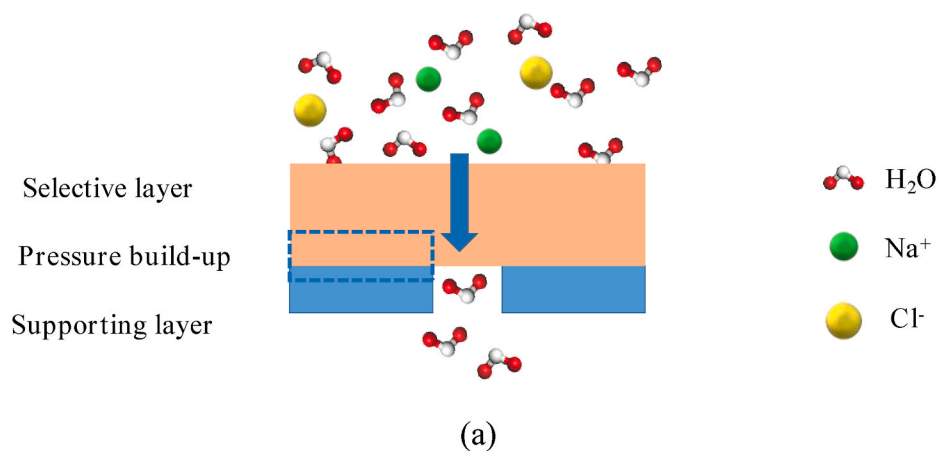


Fig. 8. A schematic diagram of the pressure build-up at the interface between the selective layer and supporting layer(a); cross-section of the PVA/PVDF membrane (b) and PVA/NC-PAN (c).

$88.4 \times 10^5$  L/(m<sup>2</sup>·h bar), indicating that the NC layer increases the gas transport resistance. Note that, the NC-PAN membrane performance is still 3.9 times higher than the PVDF membrane. Since the difference of viscosity between N<sub>2</sub> and water vapor may cause some errors in the estimation of the transport resistance of the PV composite membrane. We correlate the water vapor permeance of the substrate with pressure using the viscous flow model as described in the Supporting Information. The result indicates that the estimated water vapor flux is about 3.1 times lower than the N<sub>2</sub> flux because viscosity of water vapor is higher. If ignoring the transport resistance of the PVA selective layer, the theoretical maximum water fluxes for the PVDF, NC-PAN nanofiber and PAN

nanofiber membrane are 152.02 kg/(m<sup>2</sup>·h), 655.32 kg/(m<sup>2</sup>·h) and 2201.88 kg/(m<sup>2</sup>·h), respectively, according to the viscosity flow relationship between the water vapor flux and the *trans*-membrane pressure (the estimating process is described in Supporting Information). Therefore, the water fluxes of the PAN nanofiber based composite membranes shall be higher than the PVDF based composite membrane.

This distinct difference at PV performance can be explained by the pressure build-up at the interface between the selective layer and substrate. By applying the solution-diffusion model to a PV composite membrane [40–43], water molecule first dissolves in the dense selective layer, diffuse through the top selective layer, and finally desorbs as

**Table 2**

The pressure build-up of composite PV membranes.

Composite PV membranes	PVA layer thickness ( $\mu\text{m}$ )	Water flux ( $\text{kg}/\text{m}^2\cdot\text{h}$ )	Water vapor flux ( $\times 10^3 \text{ L}/\text{m}^2 \text{ h}$ )	Pressure build-up (kPa)
PVA/PVDF	0.88	$70.4 \pm 2.5$	$87.6 \pm 3.1$	4.01
PVA/ Hydrophobic PAN	3.50	$112.3 \pm 12.6$	$139.7 \pm 15.7$	0.63
PVA/NC-PAN	3.78	$110.9 \pm 5.1$	$138.0 \pm 6.3$	1.66

water vapor at the top surface of the porous substrate. However, the permeation of the water vapor will be restricted at uncoherent or dead-end hole regions of the support layer, and thus a pressure build-up of water vapor is produced at the interface between the bottom surface of dense selective layer and the top surface of the support layer as shown in Fig. 8a. Supposing there is no intrusion of the selective layer into the substrate, we can estimate the gas transport property by the resistance model proposed by Henis and Tripodi using Eq. (6) [44]. As listed in Table 2, a water vapor flux of  $87.6 \pm 3.1 \times 10^3 \text{ L}/(\text{m}^2\cdot\text{h})$  corresponds to a pressure build-up of 4.01 kPa of the PVA/PVDF composite membrane. Whereas for the PVA/PAN nanofiber and PVA/NC-PAN nanofiber membranes, the much higher water vapor fluxes of  $139.7 \pm 15.7 \times 10^3 \text{ L}/(\text{m}^2\cdot\text{h})$  and  $138.0 \pm 6.3 \times 10^3 \text{ L}/(\text{m}^2\cdot\text{h})$  correspond to the less pressure build-ups of 0.63 kPa and 1.66 kPa, respectively, which are only 2.09% and 5.5% of the saturate water vapor pressure of 30.08 kPa at 70 °C. The less pressure build-up indicates the higher driving force for water transport through the dense layer. Therefore, the less pressure build-up

for the PAN based substrates explains why the PVA/PAN nanofiber and PVA/NC-PAN nanofiber composite membranes have thicker PVA layers of 3.50  $\mu\text{m}$  and 3.78  $\mu\text{m}$  but show higher water fluxes than the PVA/PVDF composite membrane that has a thinner PVA layer of 0.88  $\mu\text{m}$ . These results demonstrate again that the importance of selecting a support layer with an interconnected pore structure, as illustrated in Fig. 8c.

### 3.5. Optimization of the thickness of the PVA layer

After optimizing the PAN membranes structure, the thickness of the PVA layers are gradually reduced as far as they are defect-free to further enhance the water fluxes of the PAN based composite membranes. Owing to the high rejection to PVA (80.6%) of the NC-PAN substrate, a thin PVA layer of  $\sim 0.70 \mu\text{m}$  TFC membrane is fabricated while the PVA/Hydrophobic PAN nanofiber composite membrane with a similar PVA layer thickness has many surface defects (Fig. S8). Therefore, the NC-PAN nanofiber membrane is selected as an ideal substrate and the PVA/NC-PAN composite membranes with the PVA layer thicknesses of 3.78  $\mu\text{m}$ , 1.26  $\mu\text{m}$  and 0.70  $\mu\text{m}$  are prepared (Fig. 9a, b, c). Because of the

**Table 3**

The roughness of the TFC PV membrane surface.

Membranes	$R_a$ (nm)	$R_q$ (nm)	$R_{max}$ (nm)
Pristine PAN	390	539	3567
NC/PAN	15.9	20.9	145
PVA/NC/PAN	4.71	5.81	31.3

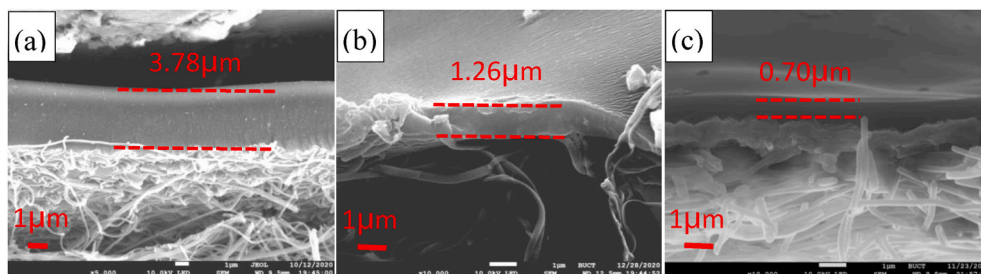


Fig. 9. The SEM images of the cross-section of the composite PV membranes with selective layer thicknesses of 3.78  $\mu\text{m}$  (a), 1.26  $\mu\text{m}$  (b), and 0.70  $\mu\text{m}$  (c).

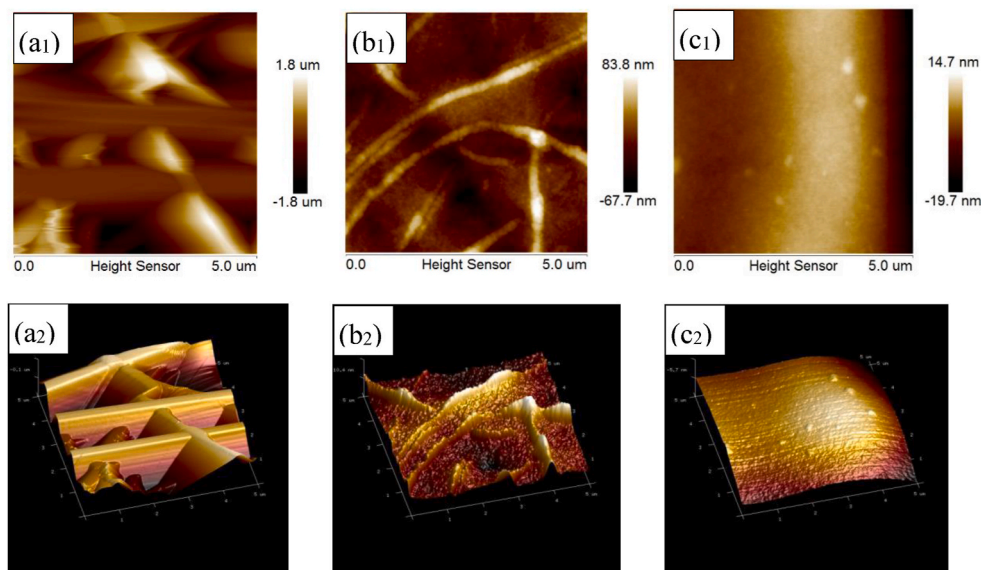
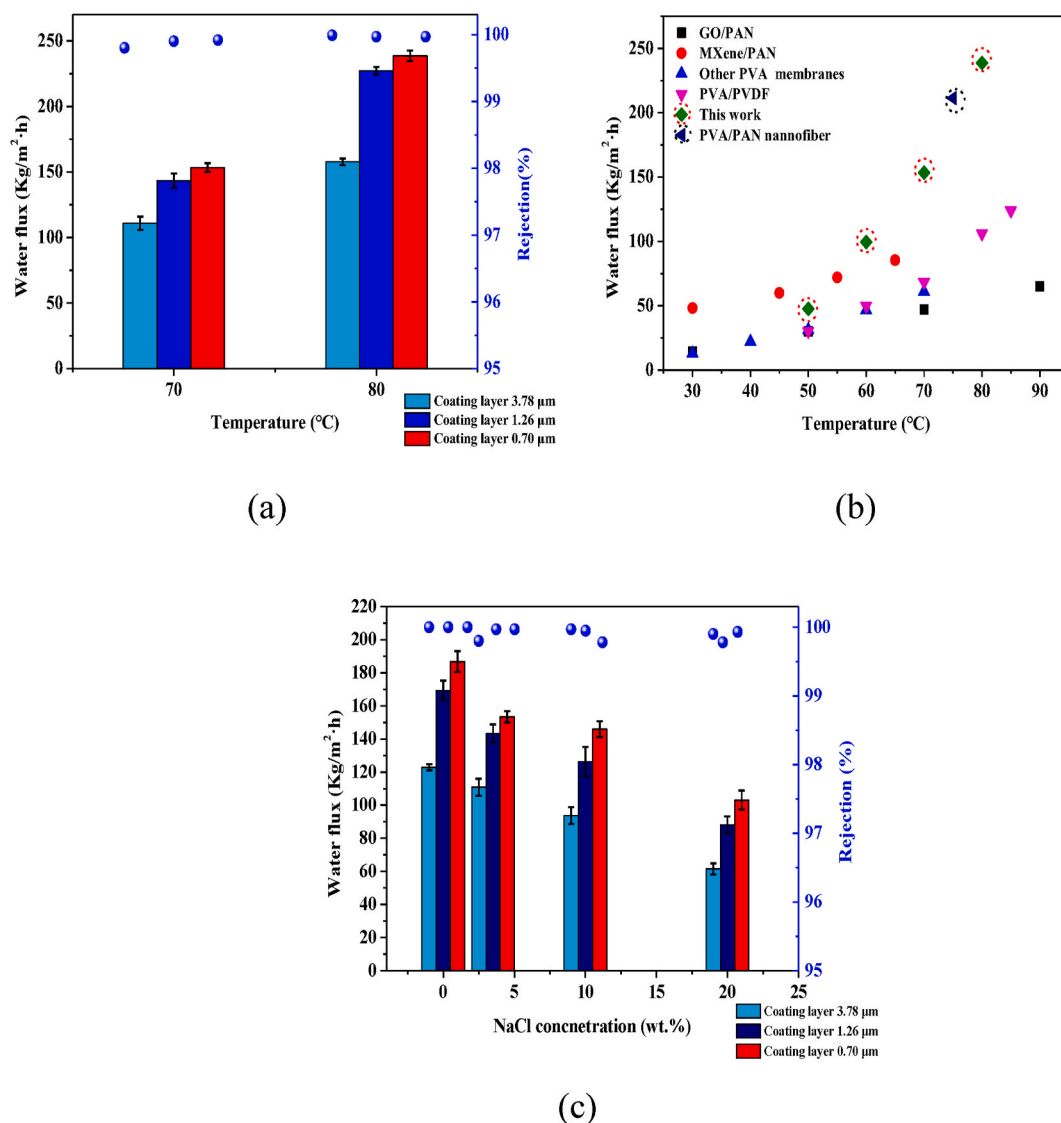


Fig. 10. AFM morphology of the PVA/NC-PAN membrane with a 0.70  $\mu\text{m}$  PVA layer.



**Fig. 11.** The PV composite membrane performances of the PVA/NC-PAN composite membranes with different PVA layer thicknesses using a 3.5 wt% NaCl solution as feed at 70 °C and 80 °C (a); a comparison of desalination performances of our PV membranes with the reported membranes (b); and comparison of the desalination properties for feed solutions with a NaCl concentration of 0–20 wt% (c).

smooth dense PVA layer covers the NC-PAN surface completely, the surface morphology of the composited membrane has been changed (Fig. 10). Table 3 lists the values of  $R_a$ ,  $R_q$  and  $R_{max}$  of the PAN nanofiber membrane, NC-PAN nanofiber composite and the PVA (0.7 μm)/NC-PAN nanofiber composite membrane. Clearly, the roughness gradually decreases after the NC and PVA layers are coated on the PAN nanofiber surface. This further proves that the thin PVA layer has deposited on the top surface of NC-PAN successfully.

### 3.6. Pervaporation desalination performance

Desalination properties of the PVA/NC-PAN composite PV membranes with different thicknesses of PVA layers are assessed using an aqueous solution comprising 3.5 wt% NaCl as feed. Fig. 11a shows that all the membranes have high salt rejections above 99.8% suggesting that the PVA layers are defect-free. Water flux increases from  $110.9 \pm 5.1$  kg/(m<sup>2</sup>·h),  $143.4 \pm 5.5$  kg/(m<sup>2</sup>·h) to  $153.4 \pm 3.4$  kg/(m<sup>2</sup>·h) at 70 °C as the PVA selective layer thickness decreases from 3.78 μm, 1.40 μm, to 0.70 μm. At a feed temperature of 80 °C, the water fluxes increase to  $159.8 \pm 2.4$  kg/(m<sup>2</sup>·h),  $227.2 \pm 2.9$  kg/(m<sup>2</sup>·h), and  $238.7 \pm 4.1$  kg/(m<sup>2</sup>·h), respectively. Comparing with the literature reported data [17–19,45],

the PVA/NC-PAN nanofiber composite membrane has the highest water fluxes. The high-water fluxes can be attributed to two reasons: the optimization of the PAN nanofibrous membranes reducing the transport resistance of the support layer and the thin layer of PVA decreasing the mass transfer resistance in the dense layer region. In summary, the PVA/NC-PAN nanofiber membrane with high performance is prepared successfully. Moreover, when desalinating a concentrated brine solution having 20 wt% NaCl, the permeation flux still reaches to  $103.1 \pm 5.8$  kg/(m<sup>2</sup>·h) with high salt rejection above 99.8%, indicating its attractive desalination property for treating concentrated brine solutions as shown in Fig. 11 c.

## 4. Conclusion

In this work, high performance of thin film composites (TFC) pervaporation membranes for desalination is fabricated by optimizing the electrospun PAN nanofiber support layer structure and thickness of selective layer. To adjust the structures of the PAN nanofiber membrane, simple techniques of hydrophobic surface modification and depositing a nanofiber cellulose (NC) layer have been attempted. Due to the reduced surface pores size diameter after coating the NC layer, a defect-free PVA/

NC-PAN composite membrane with a PVA layer of 0.70  $\mu\text{m}$  has been prepared, which exhibits a water fluxes of  $238.65 \pm 4.05 \text{ kg/m}^2\cdot\text{h}$  when desalinates a 3.5% wt. NaCl solution at 80 °C. For treating a high concentrated brine of 20 wt% NaCl solution at 70 °C, the water flux reaches to  $103.1 \pm 5.8 \text{ kg/m}^2\cdot\text{h}$  with a high salt rejection above 99.8%. Hence, the PVA/NC-PAN composite membrane is very promising for concentrated brine solution reclamation.

### Declaration of competing interest

The authors declare that they have no known competing financial interests or personal relationships that could have appeared to influence the work reported in this paper.

### Acknowledgement

This research is funded by National Natural Science Foundation of China (51773011).

### Appendix A. Supplementary data

Supplementary data to this article can be found online at <https://doi.org/10.1016/j.memsci.2021.119672>.

### References

- [1] M.A. Shannon, P.W. Bohn, M. Elimelech, J.G. Georgiadis, B.J. Mariñas, A. M. Mayes, Science and technology for water purification in the coming decades, *Nature* 452 (7185) (2008) 301–310.
- [2] N. Ghaffour, T.M. Missimer, G.L. Amy, Technical review and evaluation of the economics of water desalination: current and future challenges for better water supply sustainability, *Desalination* 309 (2013) 197–207.
- [3] M. Elimelech, W.A. Phillip, The future of seawater desalination: energy, technology, and the environment, *Science* 333 (2011) 712–717.
- [4] T. Tong, M. Elimelech, The global rise of zero liquid discharge for wastewater management: drivers, technologies, and future directions, *Environ. Sci. Technol.* 50 (2016) 68466–68855.
- [5] W. Kaminski, J. Marszałek, E. Tomczak, Water desalination by pervaporation-Comparison of energy consumption, *Desalination* 433 (2018) 89–93.
- [6] C. H. H. Jeong, K.W. Jeong, S.H. Choi, Improved productivity of the MSF (multi-stage flashing) desalination plant by increasing the TBT (top brine temperature), *Energy* 107 (2016) 683–692.
- [7] R. Castro-Muñoz, Breakthroughs on tailoring pervaporation membranes for water desalination: a review, *Water Res.* 187 (2020) 116428.
- [8] Q.Z. Wang, N. Li, B. Bolto, M. Hoang, Z.I. Xie, Desalination by pervaporation: a review, *Desalination* 387 (2016) 46–60.
- [9] P. Swenson, B. Tanchuk, A. Gupta, W. An, S.M. Kuznicki, Pervaporative desalination of water using natural zeolite membranes, *Desalination* 285 (2012) 68–72.
- [10] G.R. Xu, J.M. Xu, H.J. Feng, H.L. Zhao, S.B. Wu, Tailoring structures and performance of polyamide thin film composite (PA-TFC) desalination membranes via sublayers adjustment—a review, *Desalination* 417 (2017) 19–35.
- [11] F. Peng, J. Liu, J. Li, Analysis of the gas transport performance through PDMS/PS composite membranes using the resistances-in-series model, *J. Membr. Sci.* 232 (2003) 225–234.
- [12] D.F. Li, T.S. Chung, J. Ren, R. Wang, Thickness dependence of macrovoid evolution in wet phase-inversion asymmetric membranes, *Ind. Eng. Chem. Res.* 43 (2004) 1553–1556.
- [13] B. Liang, K. Pan, L. Li, E.P. Giannelis, B. Cao, High performance hydrophilic pervaporation composite membranes for water desalination, *Desalination* 347 (15) (2014) 199–206.
- [14] F. EjazAhmed, B. SinghLalia, R. Hashaikeh, A review on electrospinning for membrane fabrication: challenges and applications, *Desalination* 356 (2015) 15–30.
- [15] X. Wang, X. Chen, K. Yoon, D. Fang, B.S. Hsiao, B. Chu, High flux filtration medium based on nanofibrous substrate with hydrophilic nanocomposite coating, *Environ. Sci. Technol.* 39 (2005) 7684–7691.
- [16] K. Yoon, K. Kim, X. Wang, D. Fang, B.S. Hsiao, B. Chu, High flux ultrafiltration membranes based on electrospun nanofibrous PAN scaffolds and chitosan coating, *Polymer* 47 (2006) 2434–2441.
- [17] Y.L. Xue, J. Huang, C.H. Lau, B. Cao, P. Li, Tailoring the molecular structure of crosslinked polymers for pervaporation desalination, *Nat. Commun.* 11 (2020) 1461.
- [18] C. Cheng, L.D. Shen, X.F. Yu, Y. Yang, X. Li, X.F. Wang, Robust construction of a graphene oxide barrier layer on a nanofibrous substrate assisted by the flexible poly(vinylalcohol) for efficient pervaporation desalination, *J. Mater. Chem.* 5 (50) (2017) 3558–3568.
- [19] G.Z. Liu, J. Shen, Q. Liu, G.P. Liu, J. Xiong, J. Yang, W.Q. Jin, Ultrathin two-dimensional MXene membrane for pervaporation desalination, *J. Membr. Sci.* 548 (2018) 548–558.
- [20] T.L.S. Silva, S. Morales-Torres, J.L. Figueiredo, A.M.T. Silva, Multi-walled carbon nanotube/PVDF blended membranes with sponge- and finger-like pores for direct contact membrane distillation, *Desalination* 357 (2015) 233–245.
- [21] M. Khayet, C. Cococar, M.C. García-Payo, Experimental design and optimization of asymmetric flat-sheet membranes prepared for direct contact membrane distillation, *J. Membr. Sci.* 351 (2010) 234–245.
- [22] L. Zheng, J. Wang, D. Yu, Y. Zhang, Y. Wei, Preparation of PVDF-CTFE hydrophobic membrane by non-solvent induced phase inversion: relation between polymorphism and phase inversion, *J. Membr. Sci.* 550 (15) (2018) 480–491.
- [23] Y. Li, R. Yang, R. Zhang, B. Cao, P. Li, Preparation of thermally imidized polyimide nanofiltration membranes with macrovoid-free structures, *Ind. Eng. Chem. Res.* 59 (2020) 14096–14105.
- [24] J.Q. Meng, C.H. Lau, Y.L. Xue, R. Zhang, B. Cao, P. Li, Compatibilizing hydrophilic and hydrophobic polymers via spray coating for desalination, *J. Mater. Chem. A* 8 (2020) 8462.
- [25] M. Han, L. Gong, J. Wang, X. Zhang, Y. Jin, R. Zhao, C. Yang, L. He, X. Feng, Y. Chen, An octuplex lateral flow immunoassay for rapid detection of antibiotic residues, aflatoxin M1 and melamine in milk, *Sens. Actuators, B.* 292 (2019) 94–104.
- [26] E. Elemek, A. Urgancioglu, J. Dincer, A. Cilingir, Does implant-abutment interface affect marginal bone levels around implants, *Eur. J. Dermatol.* 13 (1) (2019) 47–52.
- [27] R.M. Zain, A.M. Razali, K.A.M. Salleh, R. Yahya, Image reconstruction of x-ray tomography by using image J platform, in: *AIP Conference Proceedings* 1799, 2017, <https://doi.org/10.1063/1.4972944>, 050010.
- [28] H. Sun, X. Yang, Y. Zhang, X. Cheng, Y. Xu, Y. Bai, L. Shao, Segregation-induced in situ hydrophilic modification of poly-(vinylidene fluoride) ultrafiltration membranes via sticky poly(ethylene glycol) blending, *J. Membr. Sci.* 563 (2018) 22–30.
- [29] J.M.S. Henis, M.K. Tripodi, Composite hollow fiber membranes for gas separation: the resistance model approach, *J. Membr. Sci.* 8 (3) (1981) 233–246.
- [30] B. Liang, Q. Li, B. Cao, P. Li, Water permeance, permeability and desalination properties of the sulfonic acid functionalized composite pervaporation, *Desalination* 433 (2018) 132–140.
- [31] T. Saito, Y. Nishiyama, J.L. Pataux, M. Vignon, A. Isogai, Homogeneous suspensions of individualized microfibrils from TEMPO-catalyzed oxidation of native cellulose, *Biomacromolecules* 7 (2006) 1687–1691.
- [32] Y.M. Fan, T. Saito, A. Isogai, Preparation of chitin nanofibers from squid pen  $\beta$ -chitin by simple mechanical treatment under acid conditions, *Biomacromolecules* 9 (2008) 192–198.
- [33] Y. Habibi, H. Chanzy, M.R. Vignon, TEMPO-mediated surface oxidation of cellulose whiskers, *Cellulose* 13 (2006) 679–687.
- [34] A. Isogai, T. Saito, H. Fukuzumi, TEMPO-oxidized cellulose nanofibers, *Nanoscale* 3 (2011) 71–85.
- [35] Z. Wang, H.Y. Ma, B.S. Hsiao, B. Chu, Nanofibrous ultrafiltration membranes containing cross-linked poly(ethylene glycol) and cellulose nanofiber composite barrier layer, *Polymer* 55 (2014) 366–372.
- [36] H.Y. Ma, C. Burger, B.S. Hsiao, B. Chu, Ultrafine polysaccharide nanofibrous membranes for water purification, *Biomacromolecules* 12 (2011) 970–976.
- [37] H.Y. Ma, C. Burger, B.S. Hsiao, B. Chu, Ultra-fine cellulose nanofibers: new nano-scale materials for water purification, *J. Mater. Chem.* 21 (2011) 7507–7510.
- [38] Q. Li, B. Cao, P. Li, Fabrication of high performance PV membrane by optimizing the support layer structure, *Ind. Eng. Chem. Res.* 57 (32) (2018) 11178–11185.
- [39] J.Q. Meng, P. Li, B. Cao, High-flux direct-contact pervaporation membranes for desalination, *ACS Appl. Mater. Interfaces* 11 (2019) 28461–28468.
- [40] F. Zhou, W.J. Koros, Characterization of bore pressure change effects on Matrimid fiber performance in pervaporation of acetic acid and water mixtures, *Chem. Eng. Sci.* 61 (2006) 3736–3745.
- [41] L.L. Xia, C.L. Li, Y. Wang, In-situ crosslinked PVA/organosilica hybrid membranes for pervaporation separations, *J. Membr. Sci.* 498 (2016) 263–275.
- [42] Q. Wang, N. Li, B. Bolto, M. Hoang, Z. Xie, Desalination by pervaporation: a review, *Desalination* 387 (2016) 46–60.
- [43] R. Castro-Munoz, Pervaporation: the emerging technique for extracting aroma compounds from food systems, *J. Food Eng.* 253 (2019) 27–39.
- [44] J.M.S. Henis, M.K. Tripodi, The developing technology of gas separating membranes, *Science* 220 (1983) 11–17.
- [45] R. Zhang, X. Xu, B. Cao, P. Li, Fabrication of high-performance PVA/PAN composite pervaporation membranes crosslinked by PMDA for wastewater desalination, *Petrol. Sci.* 15 (1) (2018) 146–156.